Biofilm prevention and quorum sensing interference via surface-bound peptoid

Surfaces and Interfaces 72 (2025) 107390

Contents lists available at ScienceDirect

Surfaces and Interfaces

journal homepage: www.sciencedirect.com/journal/surfaces-and-interfaces

# Biofilm prevention and quorum sensing interference via surface-bound peptoid

Francesca Gamna [a,*], Andrea Cochis [b], Gustavo Penteado Battesini Carretero [c], Jovana Curcic [d], Biljana Mojsoska [c], Milka Malesevic [d], Ziba Najmi [b], Lia Rimondini [b], Silvia Spriano [a]

[a] Politecnico di Torino, Turin, Italy
[b] Università del Piemonte Orientale (UPO), Department of Health Sciences, Center for Translational Research on Autoimmune and Allergic Diseases – CAAD, Novara, Italy
[c] Department of Science and Environment, Roskilde University, Roskilde, Denmark
[d] Institute of Molecular Genetics and Genetic Engineering, University of Belgrade, Vojvode Stepe 444a, 11042 Belgrade, Serbia

ARTICLE INFO

*Keywords:*
Peptoid
Titanium
Biofilm
Quorum sensing

ABSTRACT

The emergence of antibiotic resistance has ushered in a post-antibiotic era, highlighting the urgent need for alternative, cytocompatible antimicrobial strategies. Among these, antimicrobial peptides (AMPs) are promising to overcome antibacterial resistance being at the same time cytocompatible, but they are limited by fast enzymatic degradation. Peptoids are synthetic and bio-mimetic biomolecules that overcome the limitations of AMPs with resistance to proteolytic degradation. This study examined the antibacterial and cytocompatible peptoid GN2-Npm9 to reduce the risk of infection in titanium implants. Ti6Al4V samples were chemically pre-treated (CT) to favour osteointegration and functionalization. The zeta potential titration curves evidenced a mechanism of electrostatic attraction between the peptoid and CT substrate on the functionalized samples (CT_GN2-Npm9). XPS analysis and fluorescence microscopy confirmed the presence of the peptoid on CT_GN2-Npm9 and evidenced a uniform distribution. The peptoid was released in water with slow kinetics for at least 9 days (HPLC analyses). CT and CT_GN2-Npm9 specimens were subjected to biological assays against oral plaque collected from patients affected by periodontitis, showing a direct biofilm reduction of 60 % in comparison to CT and a specific effect towards pathogens as evidenced by proteomics studies. For investigating the mechanism of biofilm prevention, a culture of *Pseudomonas aeruginosa* was performed by conditioning the culture medium with the supernatant from the plaque test. It was observed that the biofilm of *P. aeruginosa* was significantly reduced due to a peptoid's indirect effect demonstrated by the expression of genes involved in the quorum sensing network and elastase gene (*lasB*) that resulted in down-regulation only by the supernatants from CT-GN2-Npm9 specimens.

**Statement of significance:**

This study is a groundbreaking approach to face the risk of infection of dental implants by functionalizing Ti6Al4V alloy with a synthetic peptoid (GN2-Npm9). Peptoids are promising antibacterial candidates with high chemical and biological stability, customizable structure, low cytotoxicity, broad-spectrum activity, and low resistance development. The significance of this work lies in its strategy to target biofilm formation with preventive and local action and the achievement of an antimicrobial action effective, sustained, and selective for pathogen bacteria (proteomics studies). An innovative method was implemented to investigate the mechanism of action revealing that the peptoid strongly interfered with the bacterial quorum sensing. The study offers an innovative solution to an unmet clinical need, enhancing dental and orthopaedic implants' safety and longevity.

* Corresponding author.
*E-mail address:* francesca.gamna@polito.it (F. Gamna).

https://doi.org/10.1016/j.surfin.2025.107390
Received 4 February 2025; Received in revised form 29 July 2025; Accepted 7 August 2025
Available online 13 August 2025

## 1. Introduction

Antimicrobial resistance (AMR) is a pressing global health challenge threatening the effectiveness of existing antimicrobial agents, which target specific biochemical pathways. AMR increases morbidity, mortality, and healthcare costs [1,2]. AMR is a particularly significant issue in the case of biomedical implants, where biofilm formation often necessitates explantation and leads to serious clinical complications. This is usually the case with dental and orthopaedic titanium implants. Addressing AMR requires alternative therapeutic strategies to combat resistant pathogens. Even if a wide variety of antimicrobial agents were discovered and investigated, the current limits mainly deal with cytocompatibility, effectiveness when coupled to the surface of implants, and development of AMR when an agent becomes of large use (as occurred for silver, for instance) [3]

AMPs were considered promising because of the broad spectrum of antimicrobial activity and rapid killing mechanism through the disruption of the microbial membrane, which reduces the likelihood of developing resistance[4]. The main drawback is the degradation by proteases and delivery systems need to protect AMPs and target them to the infection site in effective concentrations. They are part of the innate immune response and can have immunomodulatory effects but there is a risk that they could trigger an immune response in the host.

Peptoids, a class of biomimetic oligomers, have emerged as promising candidates for antimicrobial therapy due to their unique properties and versatile applications [5–12]. Unlike peptides, peptoids feature a backbone composed of N-substituted glycine units, endowing them with unique properties. Peptoids offer several distinct advantages over peptides, including enhanced chemical stability, resistance to proteolytic degradation, and synthesis via solid-phase methods [13]. These attributes make peptoids attractive candidates for drug discovery, molecular recognition, and materials design, where precise control over structure and function is paramount [14–16]. Additionally, the modular nature of peptoid synthesis allows for rapid exploration of diverse chemical spaces, facilitating the development of novel compounds with tailored properties [15,17,18]. Even in the realm of biomedicine, peptoids have garnered significant interest due to their biocompatibility, low immunogenicity, and interactions with biological systems [19,20]. Peptoids hold promise for applications in drug delivery, where they can enhance drug solubility, stability, and targeted delivery to specific tissues or cells [21–23]. Moreover, peptoids have demonstrated antimicrobial activity against a broad spectrum of pathogens, including bacteria, fungi, and viruses, positioning them as potential alternatives to conventional antibiotics [24–26].

Despite these advances, there is limited literature on the inhibition of biofilm formation through bacterial quorum sensing (QS) quenching using peptoids [27,28] QS is a density-dependent communication mechanism between bacterial cells, enabling them to coordinate behavior by producing and detecting chemical signaling molecules known as autoinducers[29] When cell density is high, the intracellular concentration of autoinducers increases, exposing bacterial cells to these signaling molecules. The autoinducers then pass through bacterial cell walls and membranes, triggering changes in gene expression. This process influences bacterial phenotypic behavior, enhancing pathogenesis, biofilm formation, antibiotic resistance, and the production of secondary metabolites, such as antibiotics [30]

This work aims to build upon previously published studies where a chemical surface pre-treatment of Ti6Al4V (CT) was developed for fasting osseointegration and favouring surface functionalization[31–35, 35–38]. A peptoid (GN2-Npm9) was already successfully grafted to CT samples evidencing cytocompatibility and antibacterial activity in preliminary tests against *Staphylococcus epidermidis* and *Escherichia coli* cultivated on the specimens' surface as single populations [39]. In this research work, the mechanism of surface functionalization, distribution of the peptoid on the surface, and kinetics of the release were investigated. Moreover, the peptoid's antibacterial efficacy was validated using multi-species oral microbiota isolated from the plaque of patients affected by periodontitis [39]. This approach allowed us to test the efficacy of the functionalization in a model much closer to the clinical scenario and to understand the specific effect of the peptoid on the different populations by proteomics. Lastly, a culture of *Pseudomonas aeruginosa* was performed by conditioning the culture medium with the supernatant from the previous test.

## 2. Materials and methods

### 2.1. Peptoid synthesis

GN2-Npm9 was synthesized via solid-phase submonomer chemistry method Fmoc chemistry and purified by reversed-phase HPLC, as previously described[39]. The product's identity and purity (>95 %) were confirmed by RP-UHPLC-MS analysis.

Briefly, TentaGel-S RAM swelling was carried out in DMF followed by deprotection with 20 % piperidine in DMF. Bromoacetic acid (0.6 M in DMF) and DIC (1 M in THF) were pre incubated and then added to the resin. Reaction proceeded at 40 °C for 20–30 minutes with agitation, followed by multiple DMF washes. Displacement was carried out with a 1 M solution of the desired primary amine in NMP or DMF. The reaction was carried out at 40 °C for 60 minutes. Every step was followed by extensive DMF washing. After the final displacement, resin was thoroughly washed with DMF and DCM, dried, and stored at −20 °C until cleavage. Cleavage and side-chain deprotection were achieved using a TFA-based cocktail (e.g., 50 % TFA, 45 % DCM with TIPS and water) for 30 minutes with shaking. The resin was then filtered, rinsed, and the solvent was evaporated. The resulting peptoid oil was redissolved and analyzed by HPLC-MS. Purification of crude peptoids was performed using reverse-phase preparative HPLC (250 × 10 mm, C18 column) with a gradient of 15–60 % acetonitrile in water containing 0.1 % TFA. Fractions with ≥95 % purity, confirmed by analytical HPLC-MS, were pooled, lyophilized, and stored as dry powder at −20 °C.

Fig. 1 shows the structure of the native peptide and the corresponding peptoid GN2-Npm9, highlighting the design relationship between the two molecules.

### 2.2. Sample preparation

The preparation of the samples involved cutting titanium cylindrical bars (ASTM B348, Gr5, Titanium Consulting and Trading, Buccinasco, Italy) into disks with a diameter of 10 mm and a thickness of approximately 2 mm. The surfaces of the specimens were polished using silicon carbide (SiC) abrasive papers of increasing grit sizes, up to 4000 grit. To eliminate contaminants, the polished disks underwent cleaning in acetone for 5 minutes, followed by two cycles of immersion in ultrapure water for 10 minutes each, utilizing an ultrasonic bath. These polished samples, designated as MP, were used as controls.

The MP samples were further subjected to a chemical treatment using a previously described standard and patented method [40]. In this procedure, the samples were immersed in hydrofluoric acid at room temperature, followed by thorough washing and treatment with hydrogen peroxide. The chemically treated specimens were labeled CT.

### 2.3. Surface functionalization

Before functionalization, the treated samples were exposed to UV irradiation for 1 hour to remove adventitious contaminants, physically adsorbed water, and activate the surface. A solution containing PBS and GN2-Npm9, at a concentration of 1 mg/ml, was prepared using magnetic stirring for 5 minutes. The solution was subsequently filtered through a sterilized syringe (0.2 nano filter) to avoid bacterial contamination. After UV exposure, CT samples were carefully placed on a petri dish with a drop of 100 μL of solution on the sample surface, making sure that the solution covered the entire surface, and let them

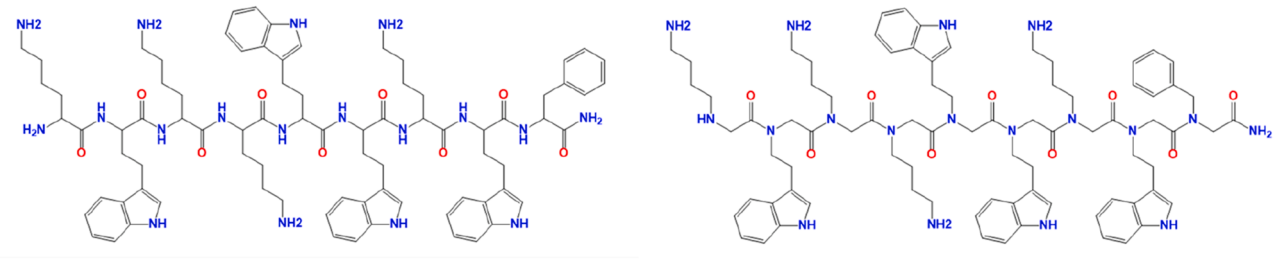

**Fig. 1.** Chemical structures of the native peptide (left) and the corresponding peptoid GN2-Npm9 (right). The peptoid was rationally designed based on the native peptide backbone, with substitution of side chains via solid-phase submonomer synthesis to enhance stability and bioactivity.

dried in incubator at 37 °C.

### 2.4. Surface characterization

#### 2.4.1. XPS

XPS spectra were collected using a monochromatic Al Kα X-ray source, with the system operating at a spot size of 100 nanometers. Both survey and high-resolution spectra were acquired to enable quantitative analysis of surface chemical composition and to determine the chemical states of Ti, Al, V, O, C, and N. The spectra were calibrated by referencing the C1s peak of hydrocarbons as an internal standard, set at a binding energy of 284.80 eV.

#### 2.4.2. Confocal Microscopy

Advanced surface imaging of the functionalized samples was performed using a confocal microscope (Zeiss LSM900). This microscope is equipped with fluorescence filters, allowing for the detection and mapping of the auto-fluorescent peptoid present on the functionalized surfaces

#### 2.4.3. Zeta Potential

The Litesizer 500 instrument was utilized to measure the zeta potential of the peptoid in an aqueous suspension. The analysis was carried out using two cuvettes, each equipped with electrodes to apply an electric field to the solution. A peptoid solution with a concentration of 0.5 mg/mL was prepared, and the zeta potential was determined as a function of pH in a 0.001 M KCl electrolyte solution. To obtain the zeta potential profile, measurements were performed at pH values of 3, 5, 6.7, 8, 9, 9.5, and 10. The starting pH was approximately 6.5 and was adjusted using either 0.05 M HCl or 0.05 M NaOH..

#### 2.4.4. Release test

The stability of the peptoid adsorbed onto the CT surface was assessed through a time-dependent release test conducted in an aqueous medium. For this purpose, 3 CT_GN2-Npm9 samples were used, each immersed in 2 mL of water. The samples were positioned inside tubes with the treated surface facing upward, and the release of the peptoid was analyzed at specific intervals: 3 hours, 24 hours, 48 hours, 5 days, and 9 days. During the experiment, the tubes were maintained at a constant temperature of 37 °C. After each time interval, the sample was transferred to a new container with fresh water to continue the release process. The total release was determined by summing the concentrations recorded at each interval.

#### 2.4.5. High Performance Liquid Chromatography coupled to mass spectrometry (HPLC-MS)

A stock solution of GN2-Npm9 peptoid was prepared in MilliQ water at a concentration of 2.0 mg/mL. This stock solution was then diluted in water to create a series of calibration standards covering 0.781 to 12.5 μg/mL concentration range. Standard curve and release test samples, taken in triplicate, were filtered through 0.22 μm and analyzed without further processing. The HPLC conditions were set as follows: Reverse Phase Chromatography C18 Kinetex column with 100 × 2.1 mm dimensions and 2.6 μm particle size (Phenomenex) was used. The mobile phase consisted of a Water and Acetonitrile mixture (90:10, v:v) with 0.1 % Trifluoracetic acid (TFA) (solvent A), and Acetonitrile with 0.1 % TFA (solvent B). The system was equilibrated running solvent A, at 0.5 mL/min, for 2 minutes. The gradient was set to 0 %-5 % B from 0 to 2.5 minutes, 5 %-65 % B from 2.5 to 8.5 minutes, 65 %-100 % B from 8.5 to 10 minutes, constant at 100 % B from 10 to 11 minutes, 100 %-0 % B from 11 to 12.5 minutes. The flow rate was set to 0.5 mL/min, the injection volume to 15 μL, and the column temperature to 40 °C. Reequilibration was performed at 0 % B for 3 minutes at 0.7 mL/min flow rate. Between every sample, a blank was run to ensure no residual signal from previous analysis. For the MS parameters, a Thermo LTQ mass spectrometer with electrospray ionization (ESI) in positive mode was used. The capillary temperature was set to 350 °C and the spray voltage to 2.2 kV. The sheath gas flow rate was adjusted to 35 arb and the auxiliary gas flow rate to 10 arb. The scan range was m/z 330-2000, with a resolution of 140.000 at m/z 330, an AGC target of 3e4, and a maximum injection time of 200 ms. Qualitative analysis was focused on the GN2-Npm9 ions MH+1 (1477.85 m/z), MH+2 (739.43 m/z), MH+3 (493.29 m/z), and MH+4 (370.22 m/z), eluted between 4.5 and 5.5 minutes. Sample detection aiming peak integration and quantification was made with a photo-diode array detector registering full UV-visible absorption spectra (200 to 800 nm). For that matter, chromatograms were generated by integrating the signal around 280 ± 2 nm, corresponding to the absorption of the four tryptamine residues of GN2-Npm9.

Obtained chromatograms were analyzed using the software Freestyle version 1.8 (Thermo Fisher Scientific) by integrating the UV abortption signal of all GN2-Npm9 for each different sample. The standard curve was used to determine the concentration of GN2-Npm9 peptoid in the samples, taken in triplicate, ensuring that the sample concentrations fell within the range of the calibration curve.

### 2.5. Biological evaluation

#### 2.5.1. Oral plaque collection

Dental plaque samples from 3 patients with periodontitis were collected at the Dental Clinic of the Maggiore Hospital in Novara using a non-invasive and non-surgical procedure, following the patient's informed consent according to the World Medical Association Declaration of Helsinki[41] The dental plaques were obtained by gently scraping the supra-gingival regions of premolars or molars with sterile Gracey curettes [42,43]. The collected samples were transferred under aseptic conditions to the Laboratory of Tissue Engineering and Biomedical Evaluation (INNOVATION Lab) at the University of Piemonte Orientale, Novara, Italy. The plaques were immediately cultured in tubes containing 30 mL of cooked meat medium (CMM, Merck, Darmstadt, Germany) and incubated under anaerobic conditions (Baker Ruskinn Concept 400 Workstations) at 37 °C. The bacteria were used immediately after reaching the exponential growth phase to preserve the original bacterial population. The collected plaques were then

divided into two parts for different experiments: 1) Direct contact with the samples (MP, CT, and CT_GN2-Npm9) to evaluate biofilm formation of oral plaque on the samples' surfaces (will be explained in Section 2.4.2); 2) Filtration through a 0.22 μm filter to remove bacterial strains, followed by immersion of the samples in 1 mL of the filtrate and incubation for 24 hours. This step allowed the release of the peptoid GN2-Npm9 from the CT_ GN2-Npm9. The resulting filtrate included the released peptoids, was referred to as 'conditioned supernatants', and was used to evaluate the indirect effect of the peptoids against *P. aeruginosa* MMA68 (will be explained in Section 2.4.4).

### 2.5.2. Specimens' infection and biofilm formation by oral microbiota

After 24 hours of cultivation in cooked meat broth and reaching the exponential phase, the plaque bacterial suspension was adjusted to a final concentration of $1 \times 10^5$ CFU (colony-forming unit)/mL (corresponding to an optical density of 0.001 at 600 nm using a spectrophotometer) and used to directly infect the specimens by adding 300 μL for each disk. After 24 hours of incubation under anaerobic conditions, samples were rinsed with a sterile phosphate-buffered saline (PBS), to eliminate bacteria not genetically predisposed to biofilm formation. The metabolic activity of the surface-adhered bacteria (biofilm) was evaluated using the AlamarBlue colorimetric assay (ready-to-use solution, Thermo Fisher Scientific, Milan, Italy). Briefly, a solution of AlamarBlue reagent (0.0015 % in PBS) was added to each sample and incubated in the dark at 37 °C for 4 hours. Following incubation, 100 μL of metabolized AlamarBlue reagent was transferred to a black 96-well plate, and fluorescence signals were measured using a spectrophotometer (Spark, Tecan Trading AG, Mannedorf, Switzerland) with an excitation wavelength of 530 nm and an emission wavelength of 590 nm. Results were reported as Relative Fluorescent Units (RFU). Additionally, the morphology of the surface-adhered bacteria and biofilm aggregates was visualized using Scanning Electron Microscopy (SEM, JSM-IT500, Jeol, Japan). Samples were fixed overnight with 2.5 % glutaraldehyde at 4 °C and dehydrated through an ethanol gradient (70 %, 90 % for 1 hour each, and 100 % for 2 hours). They were then air-dried with hexamethyldisilazane, coated with a conductive gold layer using a smart coater (Jeol, Japan), mounted onto metal stubs, and observed by SEM.

In addition to measuring the metabolic activity of the surface-adhered bacteria and visualization of bacterial aggregates (biofilm) using SEM which demonstrated general changes in biofilm formation on the samples' surfaces, proteomics analysis was applied to specifically determine which bacterial strains in the multi-species dental plague are vulnerable to the peptoid, GN2-Npm9. The following section explains the proteomics technique.

### 2.5.3. Proteomics analysis

The phyla and species colonizing the specimens' surfaces were identified using proteomics, as previously described [42]. Briefly, proteins were extracted using a lysis buffer (8 M urea and Tris-HCl) and sonication (six cycles, 27 % amplitude, 10 seconds per cycle on ice). The protein concentration was assessed using Bradford reagent (Merck, Italy), ensuring 80 μg of protein per sample. Protein reduction was performed by adding 15 μL trifluoroethanol (TFE, 99 %) and 2.5 μL of dithiothreitol (200 mM), followed by incubation at 60 °C for 30 minutes. Proteins were then digested overnight at 37 °C with trypsin, supplemented with 10 μL of iodoacetamide (IAM, 200 mM; Merck) for cysteine blocking. The digested samples were air-dried using a speed vacuum. Proteomics analysis was carried out using an Ultra-High-Performance Liquid Chromatography (UHPLC Vanquish system, from Thermo Scientific) coupled with an Orbitrap Q-Exactive Plus (Thermo Fisher Scientific). Peptides were separated on a reverse-phase column (Accucore RP-MS, 100 × 2.1 mm, 2.6 μm particle size) at 40 °C with a 0.2 mL/min flow rate. Mass spectra were analyzed using Mascot v.2.4 (Matrix Science Inc., Boston, USA) with a 10 ppm mass tolerance and a 0.1 Da MS/MS tolerance. Peptide charge states of 2þ, 3þ, and 4þ were considered on monoisotopic mass. The Human Oral Microbiome Database V3 was applied for the analysis (false discovery rate = 1 %), and peptides were mapped to their respective taxa using the Unipept database.

### 2.5.4. Biofilm formation by Pseudomonas aeruginosa MMA83 in the conditioned supernatant

This experiment evaluated the potential of peptoids released from the CT_GN2-Npm9 samples to inhibit biofilm formation via QS quenching against a single-species bacterial strain. A multi-drug-resistant clinical isolate, *Pseudomonas aeruginosa* MMA83 (Military Medical Academy; Belgrade, Serbia) was selected for this study. The isolation process for this strain has been detailed in a previous publication[44]. Generally, *P. aeruginosa* is a Gram-negative pathogenic bacterium with well-characterized QS systems at the genetic levels, which play a critical role in its pathogenicity, including biofilm formation and antibiotic resistance[30] Since *P. aeruginosa* MMA83 was not directly in contact with the samples' surfaces, this experiment was referred to as an 'indirect assay'.

Before the experiment, a fresh subculture of *P. aeruginosa* MMA83 was prepared by cultivating the strain in Muller-Hinton Broth (MHB, Bio-Rad Laboratories, France) and incubating it at 37 °C for 24 hours. Subsequently, 900 μL of the bacterial suspension, ($1 \times 10^5$ CFU/mL) was added to the wells of a 24-well plate containing sterile coverslips. Then, 100 μL of the 'conditioned supernatants' (explained in Section 2.4.1) was added to each well (supernatant: MHB ratio = 1:10). Bacterial cells cultivated on the coverslips without the addition of the 'conditioned supernatant' served as control samples and were labeled as 'POLY'. After 24 hours of incubation, biofilm formation on the coverslips was assessed using fluorescence microscopy (ZEISS Axioscope 5, Germany, 2000 × magnification). The coverslips were gently rinsed with PBS to remove planktonic bacterial cells, and the attached biofilm was stained using the LIVE/DEAD™ BacLight™ Bacterial Viability Kits (Thermo Fisher Scientific, Milan, Italy). The fluorescence intensity of the obtained micrographs was analyzed using Fiji, an open-source distribution of the ImageJ software designed for biological image analysis (40 new). The images were converted to grayscale, and the fluorescence intensity was quantified by calculating the mean gray value, defined as the sum of the gray values of all pixels within the selected area divided by the total number of pixels.

In addition to counting the viable and attached bacterial cells on the coverslips, the QS-quenching effect of the released peptoids against *P. aeruginosa* MMA83 was analyzed using real-time quantitative polymerase chain reaction (RT-qPCR).

### 2.5.6. RT-qPCR

Three major interconnected QS systems play critical roles in the pathogenicity of *P. aeruginosa* by regulating its virulence genes: the *las* system (responsible for producing enzymes such as elastases and proteases), the *rhl* system (which produces pyocyanin and other secondary metabolites), and the *pgs* system (involved in iron acquisition and oxidative stress response)[45,46]. These QS systems are highly interconnected and do not function independently[47]. Table 1 provides a list of genes corresponding to these QS systems that were analyzed in this experiment.

RNA isolation from *P. aeruginosa* MMA83, which was exposed to the collected 'conditioned supernatants' from the samples (MP, CT, and CT_GN2-Npm9) and from POLY (bacteria cultivated without supernatant as the control), was performed using the RNeasy Mini Kit (Qiagen, Germany) following the manufacturer's instructions. The isolated RNA was purified from residual DNA using a DNA-free™ DNA Removal Kit (Thermo Fisher Scientific, Milan, Italy). The concentration and purity of the isolated RNA were assessed using the BioSpec-nano instrument (Shimadzu, Kyoto, Japan). Following the manufacturer's protocol, reverse transcription was performed using the RevertAid RT Reverse Transcription Kit (Thermo Fisher Scientific, Milan, Italy). The mixture for real-time quantification contained 2 × qPCR Universal Mix (Nippon

**Table 1**
List of the primers used in this work.

| Gene | Primer name | Sequence (5′-3′) | Length (bp) | Source |
|---|---|---|---|---|
| *lasI* | lasI_Fw | GCGTGCTCAAGTGTTCAAGG | 125 | [49] |
| | lasI_Rev | GGGCTTCAGGAGTATCTTCCTGG | | |
| *lasR* | lasR_Fw | CTGTGGATGCTCAAGGACTAC | 133 | [49] |
| | lasR_Rev | AACTGGTCTTGCCGATGG | | |
| *rhlI* | rhlI_Fw | CCATCCGCAAACCCGCTACATC | 151 | [49] |
| | rhlI_Rev | CTCCCAGACCGACGGATCGCTCGGC | | |
| *rhlR* | rhlR_Fw | GGGCGTGTTCGCCGTCCTGG | 143 | [49] |
| | rhlR_Rev | GGTATCGCTCCAGCCAGGCCTTG | | |
| *pqsA* | pqs_Fw | GACCGGCTGTATTCGATTC | 74 | [49] |
| | pqs_Rev | GCTGAACCAGGGAAAGAAC | | |
| *mvfR* | mvfR_Fw | GTCGGGACGGCTACAAGGTCG | 121 | [50] |
| | mvfR_Rev | GATTGCGCGGACCCTTGTTGAG | | |
| *pqsH* | pqsH_Fw | AGGCGAACGAGGGTATTCCT | 149 | [43] |
| | pqsH_Rev | TCAGTGGGAATCGCCCTG | | |
| *lasB* | lasB_Fw | CGCAGCGTGGAGAACGCCTA | 183 | [43] |
| | lasB_Rev | GTCGGAGAACGCTTCGTTCA | | |
| *phzM* | phzM_Fw | CCGCGACATGGTGCTGTTCTA | 170 | [43] |
| | phzM_Rev | TTCATCGCCAGCAGGAAGCG | | |
| *rhlC* | rhlC_Fw | TTCCTGCCGGCCATCCATCTCG | 139 | [43] |
| | rhlC_Rev | AAGTGGCCGAGGCGCTGGTAG | | |
| *rpsL* | rpsL_Fw | GCAACTATCAACCAGCTGGTG | 231 | [49] |
| | rpsL_Rev | GCTGTGCTCTTGCAGGTTGTG | | |

Genetics, Dueren, Germany), FastGene IC Green, appropriate primers, cDNA, and bidestilled water. The primers for the selected genes are detailed in Table 1. qRT-PCR analysis was conducted using the 7500 Real-Time PCR System (Applied Biosystems, Waltham, MA, USA) under the following reaction conditions: initial denaturation at 95 °C for 2 minutes, followed by 40 cycles of denaturation at 95 °C for 5 seconds and annealing/elongation at 60 °C for 32 seconds. The *rpsL gene* was used as an endogenous control to normalize the obtained data using the $2^{-\Delta\Delta Ct}$ method [48]. Changes in the relative mRNA levels of the analyzing genes were determined compared to POLY as the control sample. All analyses were performed in triplicate and repeated three times.

### 2.6. Statistical analysis of data

For antimicrobial tests, 10 samples of each type were analyzed. Statistical analysis was conducted using SPSS software (v.20.0, IBM, USA). The normality and homogeneity of variance were confirmed using Shapiro-Wilk's and Levene's tests, respectively. Differences between groups were analyzed using the one-way ANOVA, followed by Tukey's post-hoc test. Statistical significance was set at p-value $< 0.05$ and is indicated by an asterisk (*).

## 3. Results and discussion

### 3.1. Surface characterizations

#### 3.1.1. XPS

To understand the chemical modifications induced by the functionalization process, XPS analyses were performed to evaluate the surface composition of the specimens. This characterization is essential to confirm the presence and nature of the peptoid layer on the titanium substrate and to assess the chemical environment of key elements.

Table 2 illustrates the surface composition of the specimens, denoted by the atomic percentage of the elements. A notable concentration of oxygen was detected in the CT sample, indicative of an oxide layer formation on its surface during the chemical pre-treatment. Furthermore, a considerable reduction in titanium content in CT_GN2-Npm9 corroborated the existence of a functionalized layer atop the sample, limiting the beam penetration into the titanium substrate. Carbon on the CT sample was due to unavoidable atmospheric contamination. Conversely, a doubled amount of carbon in the functionalized sample, in contrast to the CT sample, was attributable to the organic peptoid present on the surface. Accordingly, the nitrogen percentage experienced a notable augmentation in the functionalized sample due to the aforementioned organic peptoid. Instead, the nitrogen percentage on the surface of the CT sample, primarily resulting from adventitious contaminations, was exceedingly low and hence negligible.

**Table 2**
Atomic percentage of the elements detected on the surface of the samples CT and CT_GN2-Npm9.

| | O[%] | C[%] | Ti[%] | N[%] |
|---|---|---|---|---|
| CT | 55.4 | 26 | 14.8 | 3.8 |
| CT_GN2-Npm9 | 30.8 | 51.5 | 8.2 | 9.4 |

High-resolution spectra were acquired for carbon and oxygen in each sample; nitrogen's high-resolution spectra were exclusively obtained for the functionalized sample, given the negligible atomic percentage of nitrogen in the CT sample. In the carbon region (Fig. 2a), a predominant peak at 284.8 eV is discernible, attributed to C-C and C-H bonds, which was due to incidental carbon contamination on CT [51]. These chemical bonds are also evident in CT_GN2-Npm9, ascribed to the peptoid chain adhering to the surface. On CT, contributions at 286 eV and 289 eV can respectively be assigned to the C-O-C bond and carbonates [52]. A peak associated with carbonates in the CT specimen may be attributed to impurities. In the carbon spectrum of the CT_GN2-Npm9 specimen, the principal peak at around 284,8 is linked exclusively to carbon atoms bonded to other carbon or hydrogen atoms, identifiable within the peptoid skeleton. The peak at 286.2 eV corresponds to sp2 carbon bound to nitrogen, =C-NH, which is located within the aromatic ring of tryptophan-like residues. The peaks at 286.7 eV and 288 eV are attributed to carbon in the N-C-COOH bonds, which are found in the peptoid structure (Fig. 2c) and the double bond of the carboxylic group, respectively. The spectrum also shows a π-π* satellite at 292.7 eV, indicating the presence of aromatic rings and sp2 carbon, consistent with the chemical structure of tryptophan-like residues [53].

Regarding the oxygen spectrum, on CT, the peak corresponding to acid OH (approximately 530.7 eV) exhibited greater prominence compared with the basic OH (approximately 531.6 eV). This result confirmed the distinctive signal exhibited by CT samples, characterized by acidic OH groups present on the surface after the chemical pre-treatment [38]. Additionally, the peak at approximately 533 eV corresponds to physisorbed water [54]. The oxygen region of the spectrum of the CT_GN2-Npm9 sample was analyzed with three components. The peak at approximately 531.7 eV corresponds to the doubly bonded oxygen in the carboxyl group (O=C), while the peaks at 530.4 eV and 530.7 eV can be ascribed, respectively, to Ti-O and Ti-OH acid [55]. The signal associated with the Ti-O bond decreased in concordance with the presence of a functionalized layer. Additionally, the negligible presence of the peak attributed to the C-O bond in CT_GN2-Npm9 agreed with the absence of this bond in the peptoid's skeletal structure. The high-resolution nitrogen spectrum exhibits two discernible peaks, as illustrated in Fig. 2b. In the context of peptoids, the initial peak, characterized by a lower binding energy of approximately 400 eV, is attributed to primary amines (nitrogen within the C-NH2 group). Conversely, the subsequent peak, observed at 401.5 eV, corresponds to secondary amines (C-NH)[53,55].(Fig. 2c). The peak around 401.8 eV was attributed to $NH_4^+$ groups. This peak indicates the presence of an electrostatic interaction between the surface and the peptoid [55,56].

Overall, these results confirm the successful functionalization of the titanium surface with the GN2-Npm9 peptoid. The changes in elemental composition and chemical bonding demonstrate the presence of an organic layer, which is expected to influence the surface properties and biological interactions of the material.

#### 3.1.2. Confocal microscopy

Unequivocally, fluorescence microscopy revealed the consistent

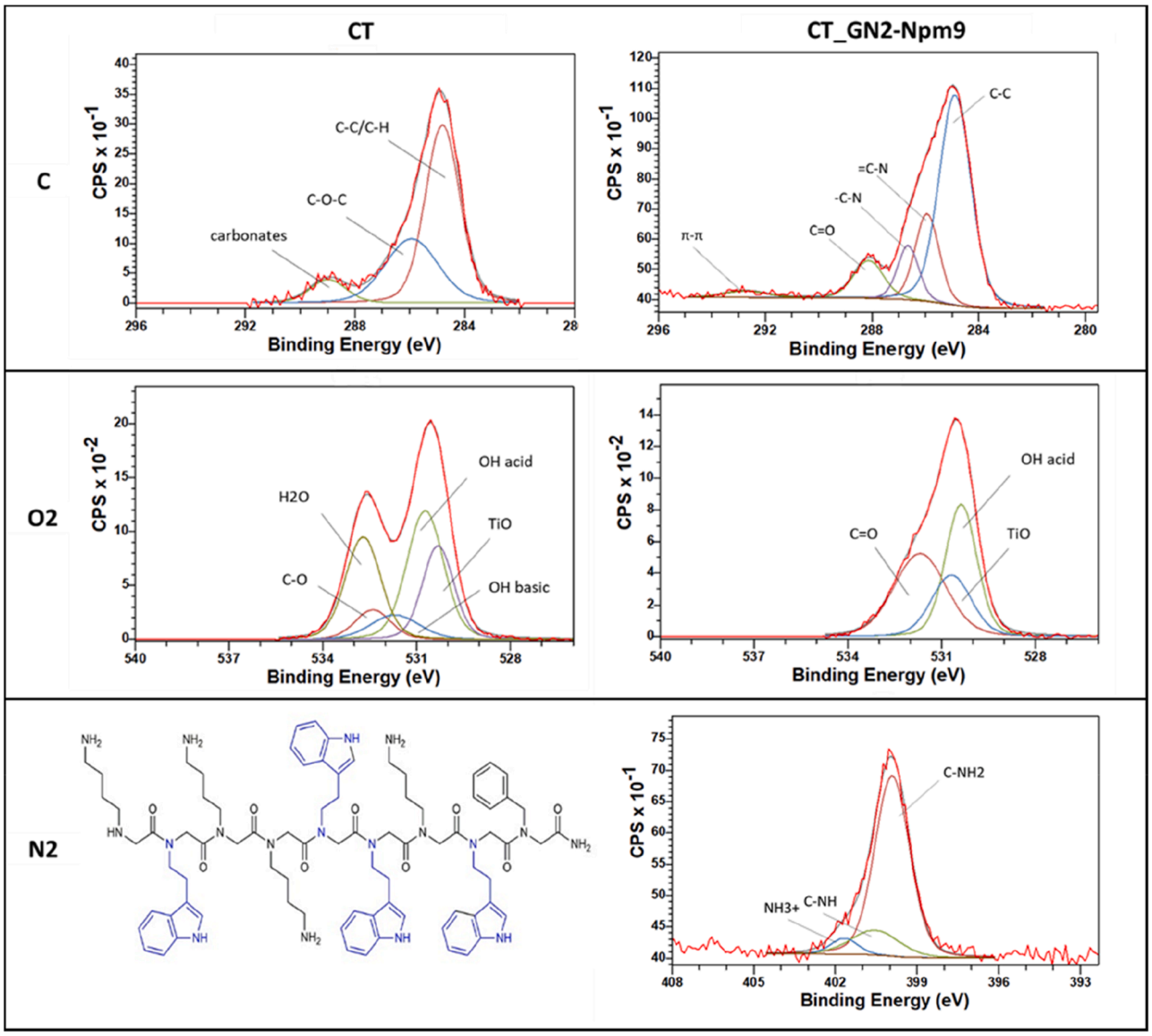


**Fig. 2.** High-Resolution spectra of a) Carbon, b) Oxygen, c) GN2-Npm9 structure and Nitrogen for CT_GN2-Npm9.

presence of red fluorescence spots distributed across CT_GN2-Npm9, providing compelling evidence of successful functionalization with the bioactive peptoid. In contrast, CT displayed no detectable fluorescence, except for certain straight lines attributed to imperfect specimen polishing.

As depicted in Fig. 3, the presence of some aggregates signifies a lack

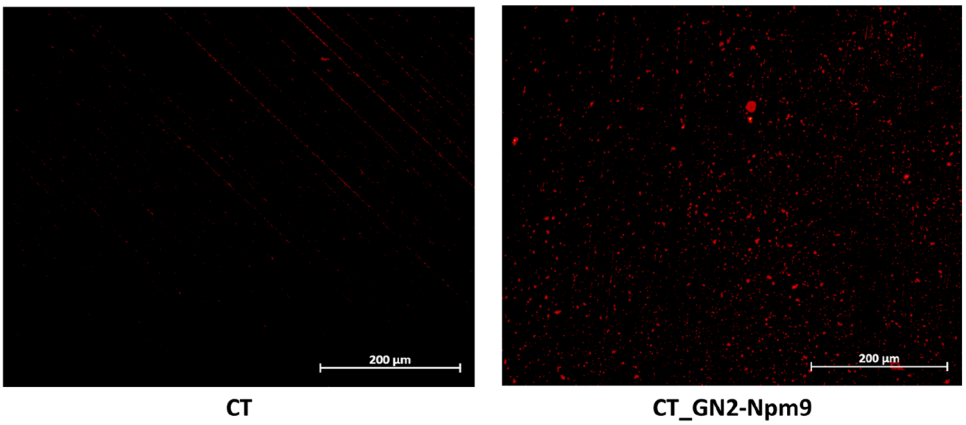


**Fig. 3.** Fluorescence microscopy images of CT and CT_GN2Npm9.

of uniform distribution of the peptoid on CT_GN2-Npm9. It agrees with the zeta potential titration curve of the functionalized specimen made in a previous work, which showed that the surface of the sample was not completely covered by the peptoid [39]

### 3.1.3. Zeta potential

The zeta potential titration curve of the GN2-Npm9 peptoid suspension exhibited distinctive features (Fig. 4). At acidic pH values, it showed a high positive zeta potential, which gradually decreased as the pH increased, although it remained positive across the entire pH range analyzed. The isoelectric point (IEP) was observed at approximately pH 9.5. This persistent positive charge was attributed to the presence of lysine residues, which carry a stable positive charge, while other components, such as the hydrophobic and apolar tryptophan-like residues, had minimal impact on the zeta potential.

The behavior of the zeta potential curve can be explained by examining the chemical structure and composition of the analogous peptide. Lysine residues, which are the positively charged elements of the peptide, have an IEP of 9.7, with pKa values of 2.2 for the alpha carboxylic group, 8.9 for the ammonium group, and 10.5 for the side chain [57]. In contrast, the other peptide component displays an IEP of 5.9, with pKa values of 2.5 for the alpha carboxylic group and 9.4 for the ammonium group. Additionally, the tryptophan-like residue is characterized by a hydrophobic and apolar side chain.

The combination of lysine and tryptophan-like residues in the formation of polypeptides results in an expected isoelectric point around pH 10. As the peptide chain lengthens, this IEP is anticipated to shift to higher values. This shift occurs independently of side chain rearrangement, as the incorporation of additional peptide units reduces the availability of carboxylic groups for deprotonation through peptide bonding. Concurrently, the number of lysine side chains increases, remaining fully available for protonation, thereby maintaining the observed zeta potential characteristics. For each pH value, three independent measurements were performed, and the standard deviation was reported to ensure statistical reliability.

### 3.1.4. HPLC

Fig. 5 shows the results of the release test of the peptoid in water. As can be observed, the release increased steadily and controllably, with an initial release after 3 hours.

This trend appears to be very interesting for the antibacterial action of the peptide. The link between the release of an antibacterial agent and its antibacterial capacity lies in the kinetics of release and the effective concentration of the antibacterial agent in the surrounding environment. Essentially, the antibacterial capacity of a compound depends on its ability to be released effectively and maintain a sufficiently high concentration to counteract bacterial growth and proliferation. Controlled and consistent release can promote greater antibacterial efficacy over time, whereas insufficient release may fail to maintain an adequate concentration to exert a significant effect on bacteria [58].

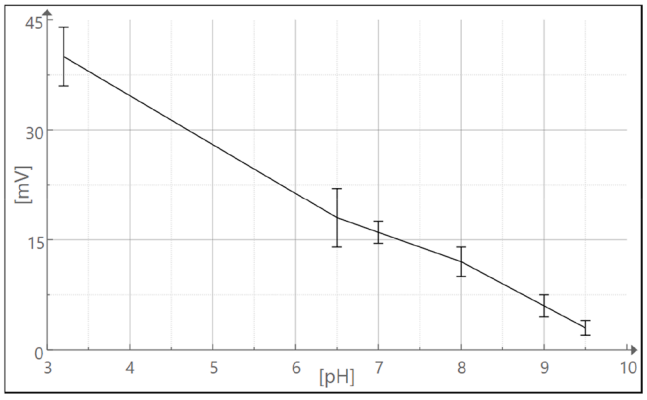


**Fig. 4.** Zeta potential titration curve of GN2-Npm9 in PBS solution. The peptoid shows a high positive zeta potential at acidic pH, which gradually decreases with increasing pH but remains positive across the entire explored range. The isoelectric point is observed above pH 9.5, reflecting the stable positive charge from lysine residues.

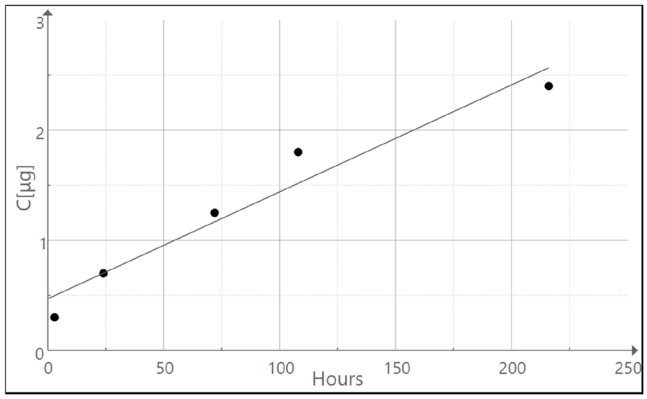


**Fig. 5.** Release test of peptoid in PBS, concentration measured through HPLC-MS over time.
Area under the curve was used to determine the release concentration using Reverse Phase Chromatography(C18 Kinetex, 100 × 2.1 mm x 2.6 µm (Phenomenex). The samples were run on a 5-65 % b gradient with water /acetonitrile mobile phase (90:10, v:v) with 0.1 % Trifluoracetic acid (TFA) (solvent A), and Acetonitrile with 0.1 % TFA (solvent B) for 12.5 minutes, flow rate 0.5 ml/min.

Unfortunately, it was not possible to quantify the amount of peptoid originally grafted and retained by the metal surface after the release test by a direct and validated method at this stage of the research. A further investigation will be performed to clarify if the remaining amount is still suitable to prevent antimicrobial activity at the different steps of the release. What we can assess is that chemisorption was able to overcome the limit of 24-48 h for the release of antibacterial agents, which is usually reported for physisorption.

## 3.2. Biological characterization

### 3.2.1. In situ oral plaque prevention

As reported in the authors' previous publication,[39] CT doped with the synthesized peptoid, GN2-Npm9, (CT_GN2-Npm9) provided a cytocompatible surface for human bone marrow mesenchymal stem cells (hMSC) to attach and spread without showing any toxicity when compared to untreated CT and Ti64 (control samples). However, a significant reduction in the metabolic activity and the viability of both Gram-positive (*Staphylococcus epidermidis*) and Gram-negative (*Escherichia coli*) bacterial strains was observed on the CT_GN2-Npm9 relative to CT and Ti64[39].This study aimed to broaden the application of the peptoid GN2-Npm9 by investigating its impact on the biofilm formation of both single-strain and multi-species bacteria, specifically by disrupting intracellular communication or QS systems.

This experiment is a more clinically relevant approach, in which a multi-species bacterial community was obtained from the oral plaque of patients suffering from periodontitis.

As demonstrated by Abusleme et al.[59] by the 16s sequencing, such conditions lead to a defined microbiota that is different from physiological and mild-pathological conditions (gingivitis) due to the relevant percentage of pathogenic species over commensal ones. Firstly, we directly infected the surface of the control (MP), microtopography (CT) and microtopography-doped with peptoid (CT_GN2-Nmp9) specimens in order to verify if the presence of the peptoid was effective in reducing the colonization of the plaque (schematized in Fig. 6a). As reported in Fig. 6b, the metabolic activity of the plaque cultivated onto the control MP was significantly higher in comparison to both CT and

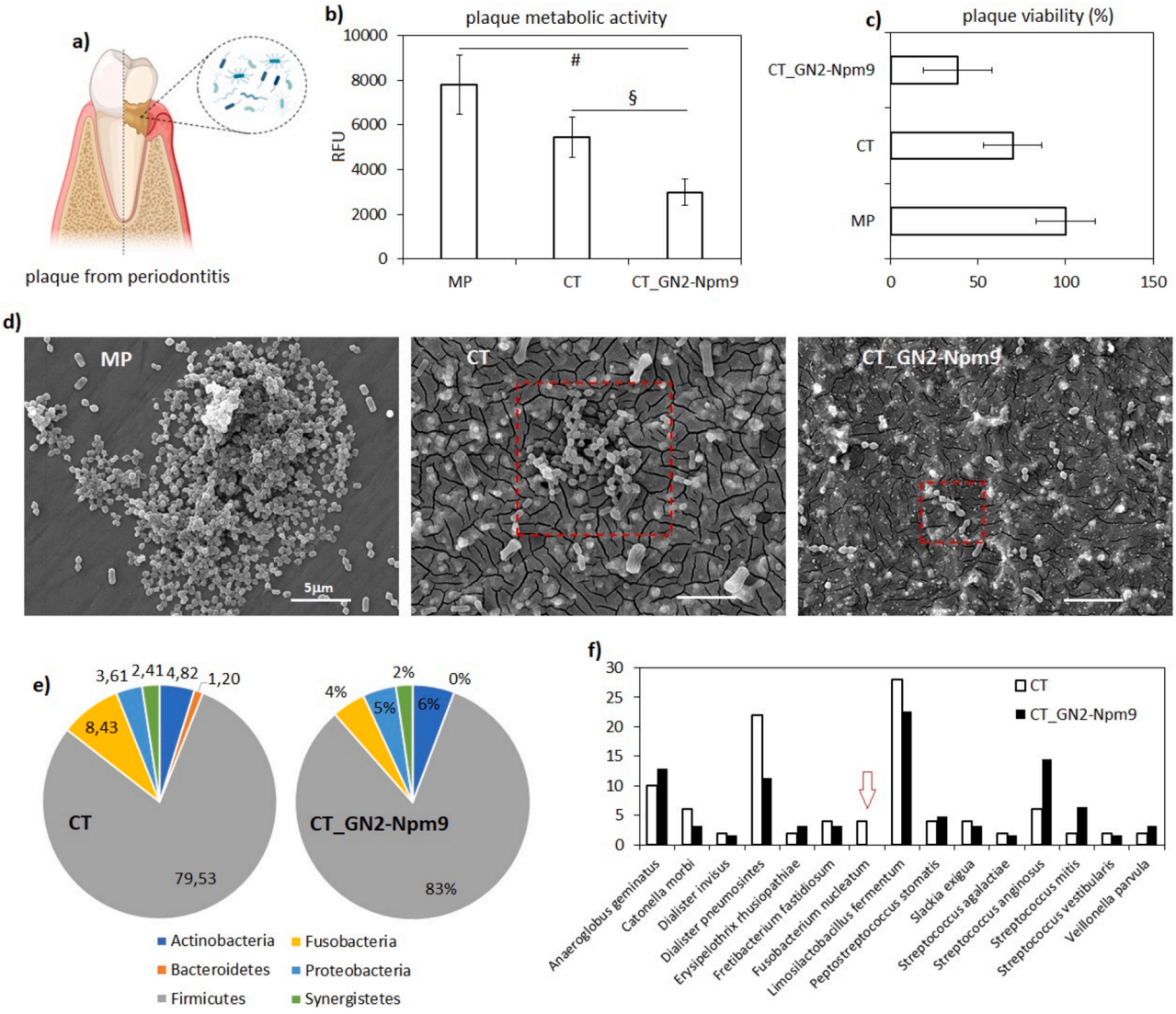


**Fig. 6.** Peptoid's antibacterial activity using oral plaque from periodontitis. (a) the metabolic activity of plaque bacteria was significantly reduced by the peptoid (CT_GN2-Nmp9) over both CT and MP controls ($p < 0.05$, indicated by # and §, respectively), (b) thus decreasing the viability of >60 % in comparison to MP controls. (d) SEM images confirmed the presence of biofilm-like aggregates onto MP and CT specimens (in the red box), while the deposition of single colonies onto CT_GN2-Nmp9 specimens. Finally, proteomics revealed the ability of the peptoid to almost eradicate the Fusobacteria phylum (e) and of the Fusobacterium nucleatum specie (f) in comparison to the CT ones. Bars represent means dev.st., replicates n = 6.

CT_GN2-Npm9 ones ($p<0.05$, indicated by #). Moreover, a further significant difference was observed by comparing the CT and the CT_GN2-Npm9 specimens to each other ($p<0.05$, indicated by §), thus confirming the bioactivity of the peptoid. As previously reported by the Authors [60,61], the presence of the CT surface treatment represents a first "physical" obstacle for bacteria due to the evidence that the microstructure reduces the anchorage points in the early adhesion phase, as well as the needle-like structures cause bacterial death due to irreversible membranes' damages. This explains the statistically significant difference between the MP control and the CT samples. The further doping with the peptoid introduced a second bioactive antibacterial agent that can efficiently bind bacterial membranes in a broad-spectrum manner (both Gram positive and Gram negative), causing irreversible damage [62]. The viability of the plaque bacteria on CT specimens was reduced by about 30 % on the MP specimens and by about 61 % on the CT_GN2-Nmp9 specimens, as summarized in Fig. 6c. Then, SEM imaging was used to confirm the metabolic results; images are reported in Fig. 6d. A dense layer of bacteria, aggregated into biofilm-like 3D structures, was visible on the MP control surfaces. A significative reduction of the surface colonization degree was noticed on CT (the few aggregates are highlighted by the red box). Differently, only a few single colonies were noticed on CT_GN2-Nmp9 specimens (highlighted by the red box) and no biofilm-like were found colonizing these surfaces.

To the best of our knowledge, this work is the first to report the potential of CT_GN2-Nmp9 in preventing bacterial colonization onto implantable metallic surfaces. Therefore, a detailed investigation of the surface doping effect on bacterial phyla and species was conducted using the proteomics technique to verify the peptoids' specific action. A comparison between the CT and the CT_GN2-Nmp9 samples was applied to focus on the peptoid's activity. Results are reported in Fig. 6e and f. Interestingly, a clear shift in the bacterial population was observed, suggesting that the peptoid may have a specific activity beyond its previously demonstrated killing effect. When phyla were investigated, the presence of the peptoid reduced Fusobacteria by >50 % (from 8.4 to 4 %) and almost eradicated the Bacteroidetes (from 1,20 to 0,1 %). This is a very promising finding as the Fusobacteria phylum includes oral-relevant pathogens such as *Fusobacterium nucleatum* which is responsible for oral infections, gastrointestinal disorders, and other severe

conditions[63]. As a confirmation, the proteomic analysis of the bacterial species (Fig. 6f) confirmed that the *Fusobacterium nucleatum* was almost completely eradicated (<0,1 %, indicated by the red arrow) by the presence of the peptoid, while it was still present in the CT samples (about 4 %).

Even though further experiments in more relevant conditions (such as saliva pre-treatment) must be conducted, it can be hypothesized that CT_GN2-Nmp9 specimens represent a promising candidate for biofunctional coating for implantable metallic materials aimed at dentistry applications.

### 3.2.2. *Indirect effect towards P. aeruginosa Biofilm formation*

After demonstrating the ability of the grafted peptoid to prevent the *in-situ* formation of biofilm from a multi-species oral plaque microbiota isolate, this study moved to evaluate in detail the effect of the peptoid GN2-Npm9 on QS quenching against a bacterial strain. Communication in multi-species bacteria (oral plaque) is much more elaborated than in a single bacterial strain because some strains of bacteria can produce autoinducers that affect other species. Additionally, distinguishing the different QS systems in multi-species bacteria was too complicated [64]. As a model single strain, *P. aeruginosa* MMA83–a clinical, multi-drug-resistant bacterium isolated from a patient–was chosen due to its well-characterized QS systems and main concerns in nosocomial-related disease,[65].

To evaluate the indirect effect of the GN2-Npm9 released from CT_GN2-Npm9 on bacterial biofilm formation, the 'conditioned supernatants' were collected after 24 hours of contact with the samples (MP, CT, CT_GN2-Npm9, and POLY; as explained in Section 2.4.1). These supernatants were diluted at a ratio of 1:10 with MHB culture medium and used to cultivate *P. aeruginosa* MMA83 (Fig. 7a). Fluorescence microscopy was employed to evaluate the biofilm formation, using the LIVE/DEAD fluorescent dye to stain bacteria. The results showed a pronounced effect of the supernatant from the CT_GN2-Npm9 sample on *P. aeruginosa* MMA83 biofilm formation compared to the MP, CT, and POLY (Fig. 7b). The fluorescent images indicated that only a sporadic number of viable bacteria attached to the coverslips were exposed to the supernatant containing released GN2-Npm9 from the CT_GN2-Npm9. In contrast, a thick biofilm layer was evident on the coverslips exposed to the supernatant from MP, CT, and POLY samples. This biofilm layer, characterized by a high intensity of green fluorescence indicating viable bacteria, highlighted the limited impact of these control supernatants on biofilm formation (Fig. 7b). Quantitative analysis of fluorescence intensity indicated the following values: MP (43.86 ± 0.06), CT (38.53 ± 0.06), Ti6Al4V (19.10 ± 1.52), POLY (29.19 ± 1.45), and CT_GN2-Nmp9 (13.61 ± 3.06). Compared to the control, the CT_GN2-Nmp9-conditioned medium led to an approximately 69 % reduction in fluorescence intensity, further confirming its inhibitory effect. Unlike the dense biofilm-like aggregates observed in the controls, the CT_GN2-Nmp9-conditioned medium yielded mostly single, randomly distributed bacterial colonies. Thereby disrupting biofilm aggregation. These findings underscore the dual anti-biofilm potential of the grafted peptoid: direct inhibition of biofilm formation on modified surfaces and indirect suppression of biofilm-promoting factors released by *P. aeruginosa*. The strong inhibitory effects demonstrated by fluorescence intensity measurements highlight the clinical potential of CT_GN2-Nmp9 in mitigating biofilm-associated infections.

To investigate the mechanism by which *P. aeruginosa* biofilm development was significantly inhibited by the supernatants from the CT_GN2-Npm9, the expression of key QS system genes (*las, rhl, and pqs*) was assessed using qRT-PCR. Table 1 presents a comprehensive list of the genes analyzed in this study. These three QS systems are highly interconnected and one system can regulate the other systems; for instance, the *las* system regulates both *rhl* and *pqs,* while the *pqs* system is linked to *rhl*[66]. The genes *lasI, rhlI, and pqsA* encode autoinducer molecules in the respective *las, rhl, and pqs* systems. These autoinducers transfer through the bacterial membrane and bind to receptor molecules (*lasR, rhlR, and mvfR)*. The resulting complexes act as transcriptional regulators of downstream genes, such as *pqsH* (enhances the production of autoinducers in the *pqs* system), *lasB* (increases elastase production), *phzM* (regulates pyocyanin modifying genes), *rhlC* (encodes rhamnosyltransferase involved in di-rhamnolipid production), *rpsL* (improve streptomycin resistance) [67–71].

Fig. 8 presents the indirect effect of GN2-Npm9 released from CT_GN2-Npm9 on the expression of autoinducers and receptor molecules in the three QS systems. The data revealed that the *rhl* and *pqs* systems are more susceptible to the peptoid than the *las* system. A statistically significant reduction ($p < 0.05$ indicated by *) in mRNA expression of *rhlI* (25 %) and *rhlR* (35 %) was observed in the

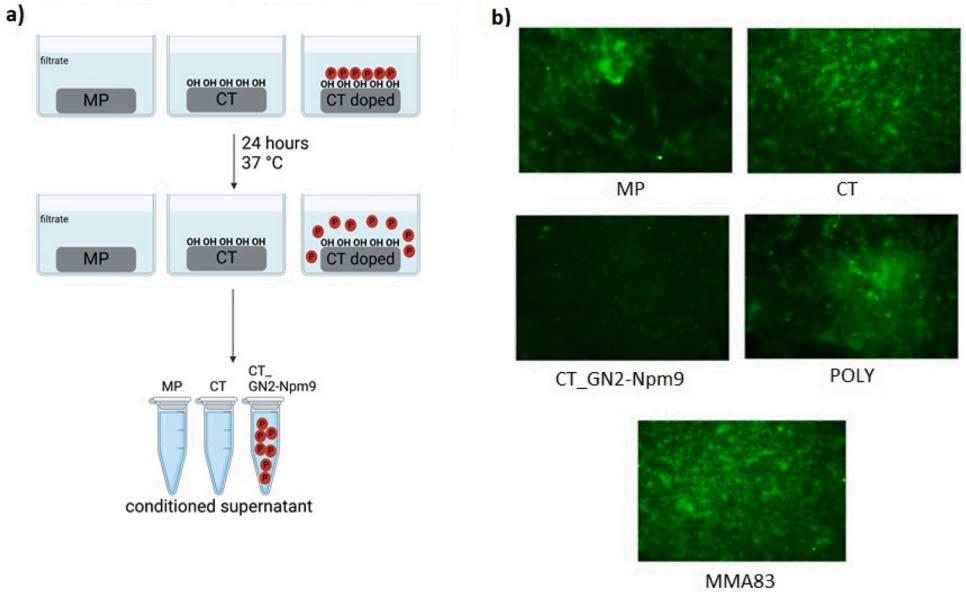


**Fig. 7.** The effect of supernatant of different Ti-based surfaces (MP, CT_GN2-Npm9, CT) and POLY on biofilm formation of multidrug-resistant clinical isolate P. aeruginosa MMA83. (a) schematic explanation of collecting the 'conditioned supernatants'; (b) fluorescence micrographs of the MMA83 biofilm (2000 × magnification).

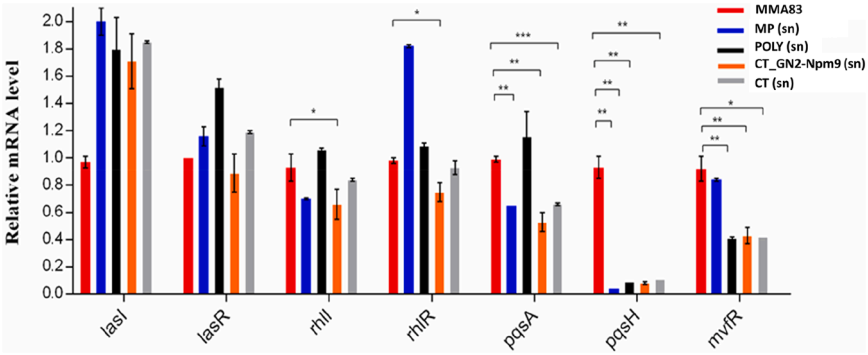


**Fig. 8.** The effect of the 'conditioned supernatants' collected from different Ti-based surfaces (MP, CT_GN2-Npm9, CT) and POLY on relative mRNA level of genes encoding autoinducer molecules and receptors in the three QS systems (las, rhl, and pqs) of P. aeruginosa MMA83. *p < 0.05, **p < 0.01, ***p < 0.001.

supernatants from CT_GN2-Npm9 in comparison to the MMA83 (control), CT, and POLY samples. A more pronounced suppression for the *pqs* system was detected, with reductions in mRNA levels of 45 % (*pqsA*), >97 % (*pqsH*), and 55 % (*mvfR*). These changes were statistically significant at $p < 0.01$ (indicated by **). Interestingly, the reduction in gene expression for *pqs* system, particularly *pqsH,* occurred across all collected supernatants, independent of the presence of the peptoid-grafted surfaces. This suggests an additional, non-specific influence on the *pqs* system that warrants further investigation (Fig. 8).

Then, the effect of the collected supernatants on the expression of functional genes regulating the behavior of *P. aeruginosa* MMA83 was evaluated by measuring the mRNA levels of *phzM, rhlC, and lasB* genes (Fig. 9). The *lasB* gene, which regulates elastase synthesis–a critical factor for biofilm maturation [72]– showed a significant reduction in expression of the *lasB* gene by 40 % when exposed to the supernatants from CT_GN2-Npm9. CT and POLY supernatants caused reductions of 40 and 30 % in the relative mRNA levels of *lasB* gene, respectively. In contrast, the MP supernatant exhibited no detectable reduction in *lasB* expression. No statistically significant reduction in the relative mRNA levels of *phzM* (regulates pyocyanin modifying genes), *rhlC* (encodes rhamnosyltransferase involved in di-rhamnolipid production) was observed in any of the supernatant-treated samples (Fig. 9).

Notably, the observed reduction in *lasB* elastase gene expression in the CT_GN2-Npm9 supernatant-treated MMA83 cannot be solely attributed to a reduction in QS, because RT-qPCR results did not demonstrate downregulation of the las system gene expression, which is a principal regulator of *lasB* gene expression [72]. However, it is important to acknowledge that *lasB* expression is not regulated solely by the *las* system. The *rhl* and *pqs* systems also play significant roles in their regulation [73]. This finding highlights the complex interplay between QS systems in controlling gene expression related to biofilm formation and virulence in P. aeruginosa.

The release profile of the peptoid by CT_GN2-Npm9, as shown in Fig. 5, is characterized by a rapid and sustained release starting from the early timepoints. This continuous elution from the surface over time plausibly contributes to the observed anti-quorum sensing and anti-biofilm effects. The released peptoid, when used to condition the culture medium for 24 hours of P. aeruginosa incubation, exhibited remarkable inhibitory effects on biofilm formation, and Fig. 10 shows a schematic representation of the proposed mechanism of GN2-Npm9-mediated QS inhibition. The hypothetical mechanism is that peptoid, GN2-Npm9, downregulates the genes encoding autoinducers and their receptors (*mvfR, pqsH, pqsA, rhlR, and rhlI*) in *P. aeruginosa*, which in turn leads to decreased expression of the elastase gene (*lasB*), a key contributor to biofilm formation in this strain These findings align with previously reported data [74,75].

Considering the poor penetration of antibiotics into biofilms and the easy spread of antimicrobial resistance genes between bacteria within the biofilm [76], preventing biofilm formation may increase the susceptibility of *P. aeruginosa* to antibiotics or phages. These results indicate that peptoids could be promising agents to prevent bacterial colonization of medical implants and impair the quorum sensing signaling network of pathogenic bacteria.

Furthermore, it has to be kept in mind that the QS signaling network of *P. aeruginosa* operates within a complex, multilayered hierarchy that includes interconnected signaling mechanisms that control gene expression in intricate ways, the full regulation of which is still unknown [77]. Few studies have explored the ability of peptoids to mimic autoinducers and disrupt QS systems in bacteria[27]. For instance, McBrayer et al., (2022) reported that a hybrid peptoid-protein analog gelatinase

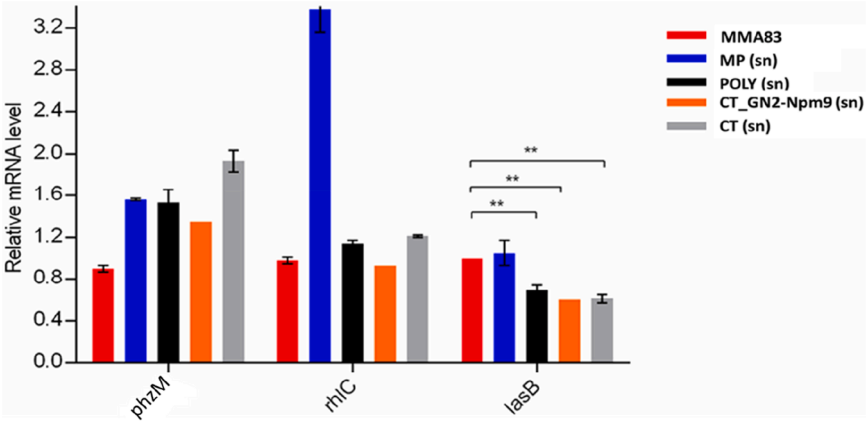


**Fig. 9.** The effect of 'conditioned supernatants' collected from different Ti-based surfaces (MP, CT_GN2-Npm9, CT) and POLY on relative mRNA level of functional genes of P. aeruginosa MMA83 which regulate bacterial phenotype. **p < 0.01.

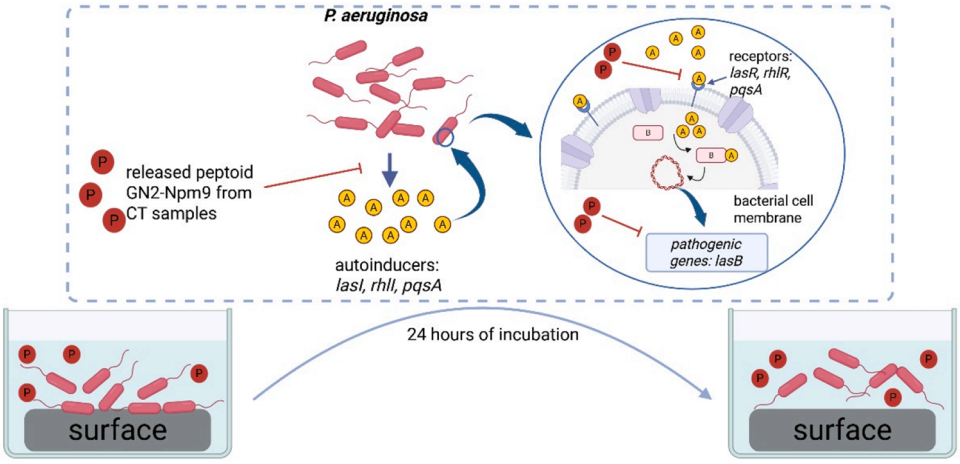


**Fig. 10.** Schematic representation of the proposed mechanisms of the released peptoid, GN2-Npm9, on the QS inhibition and as a result reduction in P. aeruginosa biofilm formation on the coverslip surfaces. Green arrows show the normal procedure of QS, and red block arrows demonstrate the effect of peptoid on the QS system.

biosynthesis activating pheromone (GBAP), could interfere with the Fsr-mediated QS system in *Enterococcus faecalis*. The Fsr system regulates genes related to virulence factors and biofilm formation [78]. Several studies have proposed that certain linear and cyclic peptidomimetics can interfere with QS by mimicking native autoinducing peptides (AIPs) and competitively inhibiting their receptors [27,79,80]. It was shown that linear peptide-peptoid hybrids can modulate the expression of agr-regulated virulence factors in Staphylococcus aureus. It is hypothesized that these peptide-peptoid hybrids adopt conformations that mimic AIP-I, thereby interfering with receptor binding and subsequent signal transduction (Karathanasi et al., 2018). Additionally, other studies have shown that synthetic peptides containing aromatic residues such as tryptophan can significantly inhibit QS-regulated virulence factors in *P. aeruginosa*. For example, in the work published by Shang and coworkers [81].Trp-containing peptides suppressed the expression of genes controlled by both the las and rhl QS systems in a dose-dependent manner. Another study further supports the notion that synthetic peptides, such as LIVRRK and LIVRHK, can act as potent QS inhibitors, significantly reducing virulence factor production in *P. aeruginosa* without necessarily exerting bactericidal effects[82]. Taken together, these findings suggest that amphipathic peptoid may exert dual activity: disrupting membrane integrity at higher concentrations, while at sub-inhibitory concentrations, mimicking native QS signals to interfere with QS receptor-ligand interactions.

In addition, it is important to note that the interaction of dental plaque bacteria incubated with the samples could have a different interaction with *P. aeruginosa* MMA83 that affects quorum sensing and virulence factor expression in MMA83. However, the exact mechanisms underlying this interaction are not yet known and require further investigation. Nonetheless, it is evident that the functionalization of chemically pre-treated (rough) titanium alloy with peptoids, owing to their anti-quorum sensing and anti-biofilm properties, stands out as the most auspicious strategy for advancing the design of innovative medical devices when compared to alternative materials.

We can state that this study introduces a significant advancement in the field of surface and interface science by demonstrating the successful functionalization of a chemically treated titanium alloy (CT) with a synthetic peptoid (GN2-Npm9) that confers dual antibacterial properties. The chemisorption mechanism was effective and allowed for a sustained release across several days. This can be explained by the high density of -OH functional groups with a strong acidic reactivity on the treated titanium surface and a positive charge on the peptoid. Unlike previous approaches that focus solely on bactericidal effects at the surface, this work provides evidence of both direct inhibition of bacterial colonization on the material surface and indirect disruption of quorum sensing mechanisms, which are essential for coordinated biofilm development. Proteomics analysis of oral microbiota provided a strain-specific insight into anti-biofilm efficacy in a clinically relevant model.

However, some limitations must be acknowledged. An analytical method suitable to quantify the amount of grafted peptoid on the surface must be developed. The study was performed in vitro, and while it used clinically relevant samples (oral plaque from periodontitis patients), in vivo validation remains necessary to confirm biocompatibility and long-term efficacy in a dynamic physiological environment. Additionally, while the quorum sensing interference was clearly demonstrated in *P. aeruginosa*, the exact molecular mechanism behind peptoid-mediated quorum quenching remains to be fully elucidated. Further investigations should also explore the response of commensal bacterial species to the functionalized surfaces to ensure microbiome balance is maintained.

## 4. Conclusions

This study successfully demonstrates the effectiveness of the synthetic peptoid GN2-Npm9 in enhancing the antibacterial properties of chemically treated titanium surfaces (CT_GN2-Npm9). The peptoid was effectively adsorbed onto titanium surfaces through electrostatic attraction, confirmed by zeta potential titration curves, XPS analysis, and fluorescence microscopy. The controlled release of GN2-Npm9 over at least nine days underscores its potential for sustained antimicrobial action. The peptoid's effect on the biofilm formation of multi-species bacterial strains was evaluated on the clinical dental plaque that was directly infected on the samples' surfaces. In addition to performing common analysis, such as the metabolic activity assessment of the surface-adhered bacteria and visualization of bacterial aggregates on surfaces, the proteomics technique was applied to determine which bacterial strains were more vulnerable to the GN2-Npm9. The results demonstrated a significant reduction in the metabolic activity and bacterial viability of surface-adhered bacteria on the surface of CT_GN2-Npm9 samples which was confirmed through visualization by SEM. Proteomics analysis showed a noticeable reduction in the phylum of Fusobacteria, particularly Fusobacterium nucleatum with $>$ 99 % biofilm formation inhibition, on the CT_GN2-Npm9 samples.

For verification of the QS quenching effect of the peptoids, P. aeruginosa MMA83 was selected as a well-studied bacterial model for QS systems and their impacts on bacterial pathogenesis. The release of GN2-Npm9 during the initial 24 hours was the principle of the experiment of biofilm formation inhibition and QS interruption against the P. aeruginosa MMA83. The fluorescent staining of bacterial aggregations on the coverslip glasses in exposure to the collected supernatant from MP, CT, CT_GN2-Npm9, and POLY showed a noticeable reduction in adherence

of bacteria in the presence of the peptoid released from CT_GN2-Npm9. The qRT-PCR results revealed a significant reduction in the mRNA level of autoinducers, particularly in rhl (rhlI and rhlR) and pqs (pqsA, pqsH, and mvfR) systems, as a result demonstrating a significant reduction in the expression (mRNA level) of lasB gene which plays an important role in biofilm formation in P. aeruginosa.

This study is among very few numbers of literature focusing on the impact of peptoids on the QS systems in bacterial strains and for the first time chemically treated titanium (CT) doped with the peptoid utilized for biofilm formation inhibition of multi-species oral plaque sample. This work is valuable for future research concerning the reduction in biofilm formation on the implants' surfaces with interruption of inter- and intra-species communications.

These findings demonstrate how a rationally designed synthetic peptoid can be integrated onto a clinically relevant titanium surface, not only to reduce microbial colonization but also to modulate bacterial communication pathways. Furthermore, the application of complementary surface analyses, combined with proteomic and gene expression studies, provided a detailed mechanistic understanding of the material–biofilm interface.

## Data availability statement

The datasets generated and analyzed during the current study are available from the corresponding author upon reasonable request. All experimental data supporting the findings of this study have been carefully validated and are stored securely to ensure reproducibility and transparency.

## CRediT authorship contribution statement

**Francesca Gamna:** Writing – review & editing, Writing – original draft, Visualization, Methodology, Investigation, Data curation, Conceptualization. **Andrea Cochis:** Writing – review & editing, Writing – original draft, Visualization, Methodology, Investigation, Data curation. **Gustavo Penteado Battesini Carretero:** Writing – original draft, Investigation. **Jovana Curcic:** Investigation. **Biljana Mojsoska:** Writing – original draft, Validation, Supervision. **Milka Malesevic:** Writing – original draft, Validation, Supervision, Data curation. **Ziba Najmi:** Investigation. **Lia Rimondini:** Supervision. **Silvia Spriano:** Writing – review & editing, Writing – original draft, Validation, Conceptualization.

## Declaration of competing interest

The authors declare that they have no known competing financial interests or personal relationships that could have appeared to influence the work reported in this paper.

## References


[1] A. R. Collaborators, "Articles Global burden of bacterial antimicrobial resistance in 2019 : a systematic analysis," vol. 399, 2022, doi:10.1016/S0140-6736(21)02724-0.

[2] S. Khalid, et al., Journal of Medicine, Surgery, and Public Health Antimicrobial resistance : Impacts, challenges, and future prospects, J. Med. Surgery Public Heal. 2 (January) (2024) 100081, https://doi.org/10.1016/j.glmedi.2024.100081.

[3] S. Kamat, M. Kumari, Emergence of microbial resistance against nanoparticles: Mechanisms and strategies, Front. Microbiol. 14 (2023), https://doi.org/10.3389/fmicb.2023.1102615.

[4] Q.Y. Zhang, et al., Antimicrobial peptides: mechanism of action, activity and clinical potential, Mil. Med. Res. 8 (1) (2021) 1–25, https://doi.org/10.1186/s40779-021-00343-2.

[5] S. A. Fowler and H. E. Blackwell, "function," vol. 7, no. 8, pp. 1508–1524, 2018, doi:10.1039/b817980h.Structure-function.

[6] P. T. Smith, M. L. Huang, and K. Kirshenbaum, "Osmoprotective polymer additives attenuate the membrane pore-forming activity of antimicrobial peptoids," vol. 103, no. 4, 2014, doi:10.1002/bip.22588.

[7] M. L. Huang, B. Y. Shin, M. A. Benson, V. J. Torres, and K. Kirshenbaum, "A comparison of linear and cyclic peptoid oligomers as potent antimicrobial agents," vol. 10016, pp. 114–122, 2012, doi:10.1002/cmdc.201100358.

[8] N. P. Chongsiriwatana et al., "Peptoids that mimic the structure, function, and mechanism of helical antimicrobial peptides," pp. 1–6, 2008.

[9] G.J. Sharples, S.L. Cobb, activity and toxicity †‡, Medchemcomm 8 (2017) 886–896, https://doi.org/10.1039/C6MD00648E.

[10] B. Mojsoska, "Peptides and peptidomimetics for antimicrobial drug design," pp. 366–415, 2015, doi:10.3390/ph8030366.

[11] B. Mojsoska, R. N. Zuckermann, and M. Microbiology, "Structure-activity relationship study of novel peptoids that mimic the structure of antimicrobial peptides," no. May, 2015, doi:10.1128/AAC.00237-15.

[12] A. M. Czyzewski, H. Jenssen, C. D. Fjell, M. Waldbrook, and E. Barron, "In Vivo, In Vitro, and in silico characterization of peptoids as antimicrobial agents," pp. 1–17, 2016, doi:10.1371/journal.pone.0135961.

[13] A. M. Webster and S. L. Cobb, "Recent advances in the synthesis of peptoid macrocycles," pp. 7560–7573, 2018, doi:10.1002/chem.201705340.

[14] S. D. Ganesh, N. Saha, and P. Sa, "Peptoids and polypeptoids : biomimetic and bioinspired materials for biomedical applications," pp. 3455–3466, 2017, doi:10.1007/s00289-016-1902-1.

[15] A. M. Clapperton, J. Babi, and H. Tran, "A field guide to optimizing peptoid synthesis," 2022, doi:10.1021/acspolymersau.2c00036.

[16] T. S. Burkoth et al., "Incorporation of unprotected heterocyclic side chains into peptoid oligomers via solid-phase submonomer synthesis," no. 13, pp. 8841–8845, 2003.

[17] S. Xuan, R.N. Zuckermann, Engineering the atomic structure of sequence-defined peptoid polymers and their assemblies, Polymer (Guildf) 202 (April) (2020) 122691, https://doi.org/10.1016/j.polymer.2020.122691.

[18] A. S. Knight, E. Y. Zhou, M. B. Francis, and R. N. Zuckermann, "Sequence programmable peptoid polymers for diverse materials applications," pp. 1–27, 2015, doi:10.1002/adma.201500275.

[19] A. Giorgio, A. Del Gatto, S. Pennacchio, M. Saviano, and L. Zaccaro, "Peptoids : smart and emerging candidates for the diagnosis of cancer, neurological and autoimmune disorders," 2023.

[20] J. Sun, Z. Li, 7. Peptoid applications in biomedicine and nanotechnology, Elsevier Ltd, 2018.

[21] J. Liu, B. Cai, L. Cui, and C. Chen, "nanomaterials : synthesis, characterization and applications," vol. 63, no. 7, pp. 1099–1112, 2020.

[22] R. Zheng et al., "Assembly of short amphiphilic peptoids into nanohelices with controllable supramolecular chirality," pp. 1–9, 2024, doi:10.1038/s41467-024-46839-y.

[23] T. P. F. Rosalba, G. D. R. Matos, C. E. M. Salvador, and C. K. Z. Andrade, "Rational design and multicomponent synthesis of lipid – Peptoid nanocomposites towards a customized drug delivery system assembly," 2023.

[24] J. Xie, et al., resistance with peptoid polymers, Nat. Commun. (2021), https://doi.org/10.1038/s41467-021-26221-y.

[25] G. Diamond et al., "Potent antiviral activity against HSV-1 and SARS-CoV-2 by antimicrobial peptoids," vol. 1, 2021.

[26] R. M. Green and K. L. Bicker, "Discovery and characterization of a rapidly fungicidal and minimally toxic peptoid against cryptococcus neoformans," 2021, doi:10.1021/acsmedchemlett.1c00327.

[27] Y. Tal-Gan, D.M. Stacy, H.E. Blackwell, N-Methyl and peptoid scans of an autoinducing peptide reveal new structural features required for inhibition and activation of AgrC quorum sensing receptors in Staphylococcus aureus, Chem. Commun. 50 (23) (2014) 3000–3003, https://doi.org/10.1039/c4cc00117f.

[28] D.N. McBrayer, U. Ghosh, M. Lella, C.D. Cameron, Y. Tal-Gan, Peptoid-Peptide Hybrid Analogs of the Enterococcus faecalis Fsr Auto-Inducing Peptide (AIP) Reveal Crucial Structure-Activity Relationships, ChemBioChem 24 (1) (2023) 1–6, https://doi.org/10.1002/cbic.202200527.

[29] S.S. Gloria Kang GJ, S.R. Ewing-Nelson, L. Mackey, J.T. Schlitt, A. Marathe, K. M. Abbas, 乳鼠心肌提取 HHS Public Access, Physiol. Behav. 176 (1) (2018) 139–148, https://doi.org/10.1038/s41579-019-0186-5.Bacterial.

[30] S.T. Rutherford, B.L. Bassler, Bacterial quorum sensing: Its role in virulence and possibilities for its control, Cold Spring Harb. Perspect. Med. 2 (11) (2012) 1–25, https://doi.org/10.1101/cshperspect.a012427.

[31] S. Ferraris, et al., Bioactive materials: In vitro investigation of different mechanisms of hydroxyapatite precipitation, Acta Biomater. 102 (2020) 468–480, https://doi.org/10.1016/j.actbio.2019.11.024.

[32] G. Riccucci, M. Cazzola, S. Ferraris, V.A. Gobbo, M. Guaita, S. Spriano, Surface functionalization of Ti6Al4V with an extract of polyphenols from red grape pomace, Mater. Des. 206 (2021) 109776, https://doi.org/10.1016/j.matdes.2021.109776.

[33] S. Ferraris, M. Cazzola, G. Ubertalli, E. Prenesti, S. Spriano, Grafting of gallic acid to metallic surfaces, Appl. Surf. Sci. 511 (October 2019) (2020) 145615, https://doi.org/10.1016/j.apsusc.2020.145615.

[34] F. Gamna, et al., The use of vitamin E as an anti-adhesive coating for cells and bacteria for temporary bone implants, Surf. Coat. Technol. 444 (May) (2022) 128694, https://doi.org/10.1016/j.surfcoat.2022.128694.

[35] M. Cazzola, et al., Grafting of the peppermint essential oil to a chemically treated Ti6Al4V alloy to counteract the bacterial adhesion, Surf. Coatings Technol. 378 (October) (2019), https://doi.org/10.1016/j.surfcoat.2019.125011.

[36] F. Gamna, et al., Grafting of alpha-tocopheryl phosphate on chemically treated Ti-6Al-4V for antibacterial bone implants, Appl. Surf. Sci. 619 (February) (2023) 156681, https://doi.org/10.1016/j.apsusc.2023.156681.

[37] V. Alessandra Gobbo, et al., Functionalization of a chemically treated Ti6Al4V-ELI alloy with nisin for antibacterial purposes, Appl. Surf. Sci. 620 (November 2022) (2023) 156820, https://doi.org/10.1016/j.apsusc.2023.156820.

[38] M. Cazzola, et al., Grafting of the peppermint essential oil to a chemically treated Ti6Al4V alloy to counteract the bacterial adhesion, Surf. Coatings Technol. 378 (September) (2019), https://doi.org/10.1016/j.surfcoat.2019.125011.

[39] F. Gamna, A. Cochis, B. Mojsoska, A. Kumar, L. Rimondini, S. Spriano, Heliyon Nano-topography and functionalization with the synthetic peptoid GN2-Npm 9 as a strategy for antibacterial and biocompatible titanium implants, Heliyon 10 (2) (2024) e24246, https://doi.org/10.1016/j.heliyon.2024.e24246.

[40] S. Spriano, S. Ferraris, and E. Vernè, "EUROPEAN PATENT SPECIFICATION 2214732," vol. 1, no. 19, pp. 1–12, 2013.

[41] E. Holstila, A. Vallittu, S. Ranto, T. Lahti, and A. Manninen, "Helsinki," Cities Engines Sustain. Compet. Eur. Urban Policy Pract.., pp. 175–189, 2016, doi:10.4324/9781315572093-15.

[42] A. D'Agostino, et al., Gallium-doped zirconia coatings modulate microbiological outcomes in dental implant surfaces, J. Biomed. Mater. Res. - Part A (August 2023) (2024) 1–12, https://doi.org/10.1002/jbm.a.37727.

[43] J. Curcic, et al., A novel thermostable YtnP lactonase from Stenotrophomonas maltophilia inhibits Pseudomonas aeruginosa virulence in vitro and in vivo, Int. J. Biol. Macromol. 264 (P1) (2024) 130421, https://doi.org/10.1016/j.ijbiomac.2024.130421.

[44] B. Jovcic, et al., Emergence of NDM-1 metallo-β-lactamase in Pseudomonas aeruginosa clinical isolates from Serbia, Antimicrob. Agents Chemother. 55 (8) (2011) 3929–3931, https://doi.org/10.1128/AAC.00226-11.

[45] A. Glessner, R.S. Smith, B.H. Iglewski, J.B. Robinson, Roles of Pseudomonas aeruginosa las and rhl quorum-sensing systems in control of twitching motility, J. Bacteriol. 181 (5) (1999) 1623–1629, https://doi.org/10.1128/jb.181.5.1623-1629.1999.

[46] C.N. Wilder, S.P. Diggle, M. Schuster, Cooperation and cheating in Pseudomonas aeruginosa: The roles of the las, rhl and pqs quorum-sensing systems, ISME J. 5 (8) (2011) 1332–1343, https://doi.org/10.1038/ismej.2011.13.

[47] Q. Li, S. Mao, H. Wang, X. Ye, 铜绿假单胞菌群体感应抑制剂的分子结构, Mar. Drugs 20 (8) (2022).

[48] K.J. Livak, T.D. Schmittgen, Analysis of relative gene expression data using real-time quantitative PCR and the 2-ΔΔCT method, Methods 25 (4) (2001) 402–408, https://doi.org/10.1006/meth.2001.1262.

[49] M. Malešević, et al., Pseudomonas aeruginosa quorum sensing inhibition by clinical isolate Delftia tsuruhatensis 11304: involvement of N-octadecanoylhomoserine lactones, Sci. Rep. 9 (1) (2019) 1–13, https://doi.org/10.1038/s41598-019-52955-3.

[50] M. Malešević, et al., Burkholderia cepacia YtnP and Y2-aiiA lactonases inhibit virulence of Pseudomonas aeruginosa via quorum quenching activity, Microb. Pathog. 149 (September) (2020), https://doi.org/10.1016/j.micpath.2020.104561.

[51] X. Zhang, S. Ferraris, E. Prenesti, E. Verné, Surface functionalization of bioactive glasses with natural molecules of biological significance, part I: Gallic acid as model molecule, Appl. Surf. Sci. 287 (2013) 329–340, https://doi.org/10.1016/j.apsusc.2013.09.151.

[52] B.V. Crist, Demo Version (87 pages) PDF handbooks of monochromatic XPS Spectra Volume 1 - The elements and native oxides (for Ag-Au), Elements 1 (March) (1999).

[53] G. Wang, et al., Environmentally friendly nanocomposites based on cellulose nanocrystals and polydopamine for rapid removal of organic dyes in aqueous solution, Cellulose 27 (4) (2020) 2085–2097, https://doi.org/10.1007/s10570-019-02944-6.

[54] M. Smith, L. Scudiero, J. Espinal, J.S. McEwen, M. Garcia-Perez, *Improving the deconvolution and interpretation of XPS spectra from chars by ab initio calculations*, vol. 110, Elsevier Ltd, 2016.

[55] A. Artemenko, et al., Reference XPS spectra of amino acids, IOP Conf. Ser. Mater. Sci. Eng. 1050 (1) (2021), https://doi.org/10.1088/1757-899X/1050/1/012001.

[56] T. Eralp, A. Shavorskiy, G. Held, The adsorption geometry and chemical state of lysine on Cu{110}, Surf. Sci. 605 (3–4) (2011) 468–472, https://doi.org/10.1016/j.susc.2010.12.001.

[57] C. Žváček, G. Friedrichs, L. Heizinger, R. Merkl, An assessment of catalytic residue 3D ensembles for the prediction of enzyme function, BMC Bioinformatics 16 (1) (2015) 1–8, https://doi.org/10.1186/s12859-015-0807-6.

[58] F. Directions, Controlled drug delivery systems : current status and, Molecules 26 (2021) 5905.

[59] L. Abusleme, A. Hoare, B.Y. Hong, P.I. Diaz, Microbial signatures of health, gingivitis, and periodontitis, Periodontol. 2000 86 (1) (2021) 57–78, https://doi.org/10.1111/prd.12362.

[60] S. Ferraris, et al., Cytocompatible and anti-bacterial adhesion nanotextured titanium oxide layer on titanium surfaces for dental and orthopedic implants, Front. Bioeng. Biotechnol. 7 (May) (2019) 1–12, https://doi.org/10.3389/fbioe.2019.00103.

[61] S. Ferraris, A. Cochis, A.C. Scalia, A. Tori, L. Rimondini, S. Spriano, Laser surface texturing of Ti-cp and Ti6Al4V alloy for the improvement of fibroblast adhesion and alignment and the reduction of bacterial adhesion, J. Mater. Res. Technol. 29 (February) (2024) 5464–5472, https://doi.org/10.1016/j.jmrt.2024.03.033.

[62] P. Saporito, B. Mojsoska, A.Løbner Olesen, H. Jenssen, Antibacterial mechanisms of GN-2 derived peptides and peptoids against Escherichia coli, Biopolymers 110 (6) (2019), https://doi.org/10.1002/bip.23275.

[63] Han Yiping, *Fusobacterium nucleatum*: a commensal turned pathogen, Curr. Opin. Microbiol. 0 (2015) 141–147, https://doi.org/10.1016/j.mib.2014.11.013.Fusobacterium.

[64] X. Zeng, Y. Zou, J. Zheng, S. Qiu, L. Liu, C. Wei, Quorum sensing-mediated microbial interactions: mechanisms, applications, challenges and perspectives, Microbiol. Res. 273 (May) (2023) 127414, https://doi.org/10.1016/j.micres.2023.127414.

[65] R. Souto, C.M. Silva-Boghossian, A.P.V. Colombo, Prevalence of Pseudomonas aeruginosa and Acinetobacter spp. in subgingival biofilm and saliva of subjects with chronic periodontal infection, Brazilian J. Microbiol. 45 (2) (2014) 495–501, https://doi.org/10.1590/S1517-83822014000200017.

[66] S.W. Miranda, K.L. Asfahl, A.A. Dandekar, E.P. Greenberg, Pseudomonas aeruginosa Quorum Sensing, Adv. Exp. Med. Biol. 1386 (2022) 95–115, https://doi.org/10.1007/978-3-031-08491-1_4.

[67] R. Rahim, et al., Cloning and functional characterization of the Pseudomonas aeruginosa rhlC gene that encodes rhamnosyltransferase 2, an enzyme responsible for di-rhamnolipid biosynthesis, Mol. Microbiol. 40 (3) (2001) 708–718, https://doi.org/10.1046/j.1365-2958.2001.02420.x.

[68] L. Huang, et al., Pyocyanin-modifying genes phzM and phzS regulated the extracellular electron transfer in microbiologically-influenced corrosion of X80 carbon steel by Pseudomonas aeruginosa, Corros. Sci. 164 (August 2019) (2020) 108355, https://doi.org/10.1016/j.corsci.2019.108355.

[69] W. Feng, et al., Piezopotential-driven simulated electrocatalytic nanosystem of ultrasmall MoC quantum dots encapsulated in ultrathin N-doped graphene vesicles for superhigh H2 production from pure water, Nano Energy 75 (June) (2020) 104990, https://doi.org/10.1016/j.nanoen.2020.104990.

[70] E. Déziel, et al., The contribution of MvfR to Pseudomonas aeruginosa pathogenesis and quorum sensing circuitry regulation: Multiple quorum sensing-regulated genes are modulated without affecting IasRI, rhIRI or the production of N-acyl-L-homoserine lactones, Mol. Microbiol. 55 (4) (2005) 998–1014, https://doi.org/10.1111/j.1365-2958.2004.04448.x.

[71] K. Vadakkan, A.K. Ngangbam, K. Sathishkumar, N.P. Rumjit, M.K. Cheruvathur, A review of chemical signaling pathways in the quorum sensing circuit of Pseudomonas aeruginosa, Int. J. Biol. Macromol. 254 (P2) (2024) 127861, https://doi.org/10.1016/j.ijbiomac.2023.127861.

[72] F. Casilag, A. Lorenz, J. Krueger, F. Klawonn, S. Weiss, S. Häussler, LasB elastase of Pseudomonas aeruginosa acts in concert with alkaline protease AprA to prevent flagellin-mediated immune recognition, Infect. Immun. 84 (1) (2015) 162–171, https://doi.org/10.1128/IAI.00939-15.

[73] H.Y. Choi, D.D. Le, W.G. Kim, Curvularin isolated from phoma macrostoma is an antagonist of RhlR quorum sensing in pseudomonas aeruginosa, Front. Microbiol. 13 (July) (2022), https://doi.org/10.3389/fmicb.2022.913882.

[74] M. Kazemzadeh-Narbat, B.F.L. Lai, C. Ding, J.N. Kizhakkedathu, R.E.W. Hancock, R. Wang, Multilayered coating on titanium for controlled release of antimicrobial peptides for the prevention of implant-associated infections, Biomaterials 34 (24) (2013) 5969–5977, https://doi.org/10.1016/j.biomaterials.2013.04.036.

[75] R. Kapoor, M.W. Wadman, M.T. Dohm, A.M. Czyzewski, A.M. Spormann, A. E. Barron, Antimicrobial peptoids are effective against Pseudomonas aeruginosa biofilms, Antimicrob. Agents Chemother. 55 (6) (2011) 3054–3057, https://doi.org/10.1128/AAC.01516-10.

[76] C. Uruén, G. Chopo-Escuin, J. Tommassen, R.C. Mainar-Jaime, J. Arenas, Biofilms as promoters of bacterial antibiotic resistance and tolerance, Antibiotics 10 (1) (2021) 1–36, https://doi.org/10.3390/antibiotics10010003.

[77] J. Lee, L. Zhang, The hierarchy quorum sensing network in Pseudomonas aeruginosa, Protein Cell 6 (1) (2015) 26–41, https://doi.org/10.1007/s13238-014-0100-x.

[78] D.N. McBrayer, U. Ghosh, M. Lella, C.D. Cameron, Y. Tal-Gan, Peptoid-peptide hybrid analogs of the enterococcus faecalis fsr auto-inducing peptide (aip) reveal crucial structure-activity relationships, ChemBioChem 24 (1) (2023) 1–13, https://doi.org/10.1002/cbic.202200527.

[79] S.A. Fowler, D.M. Stacy, H.E. Blackwell, Design and synthesis of macrocyclic peptomers as mimics of a quorum sensing signal from Staphylococcus aureus, Org. Lett. 10 (12) (2008) 2329–2332, https://doi.org/10.1021/ol800908h.

[80] G. Karathanasi, et al., Linear peptidomimetics as potent antagonists of Staphylococcus aureus agr quorum sensing, Sci. Rep. 8 (1) (2018) 1–11, https://doi.org/10.1038/s41598-018-21951-4.

[81] D. Shang, X. Han, W. Du, Z. Kou, F. Jiang, Trp-Containing antibacterial peptides impair quorum sensing and biofilm development in multidrug-resistant pseudomonas aeruginosa and exhibit synergistic effects with antibiotics, Front. Microbiol. 12 (February) (2021) 1–16, https://doi.org/10.3389/fmicb.2021.611009.

[82] M.N. Taha, A.E. Saafan, A. Ahmedy, E. El Gebaly, A.S. Khairalla, Two novel synthetic peptides inhibit quorum sensing-dependent biofilm formation and some virulence factors in Pseudomonas aeruginosa PAO1, J. Microbiol. 57 (7) (2019) 618–625, https://doi.org/10.1007/s12275-019-8548-2.